




Enhancement of room-temperature unidirectional spin Hall magnetoresistance by using a ferromagnetic metal with a low Curie temperature

Kazuto Yamanoi ^{1,*}, Hikari Semizu,¹ and Yukio Nozaki ^{1,2}

¹*Department of Physics, Keio University, Yokohama 223-8522, Japan*

²*Center for Spintronics Research Network, Keio University, Yokohama 223-8522, Japan*

 (Received 25 May 2022; revised 30 August 2022; accepted 30 August 2022; published 7 October 2022)

The unidirectional spin Hall magnetoresistance (USMR) effect is useful to detect the direction of magnetization in a ferromagnetic metal/nonmagnetic metal bilayer, which is the typical geometry used in a spin-orbit torque switching device. In this Letter, we demonstrate the enhancement of the USMR effect by reducing the Curie temperature T_C of the ferromagnetic (FM) layer in a FM/platinum bilayer. The USMR ratio was maximized when the thickness of each FM layer was consistent with the spin diffusion length. We found that the maximum USMR ratio can be doubled by replacing $\text{Ni}_{81}\text{Fe}_{19}$ ($T_C = 854$ K) with $\text{Ni}_{85}\text{Cu}_{15}$ ($T_C = 527$ K) as the FM. This enhancement of the USMR effect is attributed to an increase of electron-magnon scattering in accordance with Bloch law. We also found that the use of ferromagnets with face-centered-cubic structures, such as Ni, $\text{Ni}_{81}\text{Fe}_{19}$, and $\text{Ni}_{85}\text{Cu}_{15}$, increased the USMR effect relative to that of body-centered-cubic Fe.

DOI: [10.1103/PhysRevB.106.L140401](https://doi.org/10.1103/PhysRevB.106.L140401)

I. INTRODUCTION

Magnetoresistance (MR) effects are essential to detect not only oscillatory motion but also irreversible switching of magnetization in nanometer-scale ferromagnets, which are widely used in various spintronic devices [1]. Recently, a novel type of unidirectional MR effect, unidirectional spin Hall MR (USMR) [2–6], was observed in a ferromagnetic metal/nonmagnetic metal (FM/NM) bilayer where a spin current generated in the NM by the spin Hall effect [7–11] led to a change in the electrical resistance of the ferromagnet (FM) depending on the relative direction of the spin polarization with respect to the magnetization. Consequently, the USMR effect changes its sign by the reversal of magnetization or the flow of electric current.

There are two possible mechanisms for the USMR effect: spin-dependent (SD)-USMR and spin-flip (SF)-USMR. The former originates from the SD scattering of itinerant electrons not only in the bulk FM but also at the FM/NM interface in a manner similar to current-perpendicular-to-plane [12] and current-in-plane [13] giant MR (GMR) effects, respectively. In contrast, the SF-USMR is attributed to the resistance change of the FM layer that is caused by the creation and/or annihilation of incoherent magnons, whose magnitude depends on the relative orientation of magnetization of the FM with respect to a spin polarization of spin current generated in the nonmagnet (NM). The change in the number of incoherent magnons modulates the strength of electron-magnon scattering in the FM.

Such a USMR effect could potentially simplify a magnetoresistive random access memory (MRAM) readout system because the pinning layer, essential for a unidirectional

change in the electrical resistance of the magnetic tunneling junction, would no longer be needed. However, the ratio of the USMR effect to the electrical resistance, i.e., $\Delta R_{\text{USMR}}/R$, is still only 10^{-5} , and this is too low for practical applications.

To improve the USMR effect, attempts have been made to increase the amount of spin accumulation at the FM/NM interface. One of the promising candidates for the NM is a topological insulator (TI), where a large spin accumulation is produced owing to the momentum locking effect of electron spin at the surface [14–18]. Indeed, Khang and Hai succeeded in realizing a high USMR ratio of 10^{-3} in heterostructures consisting of a TI and a ferromagnetic semiconductor, which means matching conductivity with TIs is significant [17]. However, owing to the low Curie temperature T_C of the ferromagnetic semiconductor, it is difficult to realize a large USMR at room temperature. Moreover, poor conductivity of the TI is also unfavorable for practical application to spin-orbit torque (SOT) MRAM [19,20] because the large electrical resistance of the spin Hall channel leads to serious signal processing problems, including signal delay and distortion, and energy loss. An alternative approach to improve the USMR is to increase SD scattering at the FM/NM interface. Hasegawa *et al.* demonstrated that the USMR ratio in a cobalt (Co)/Pt bilayer could be enhanced by inserting a copper (Cu) interlayer. In this case, similar to the GMR effect seen in a Co/Cu/Co trilayer [21], the Co/Cu interface plays an important role in enhancing SD scattering. The nature of the inserted material strongly influences the FM.

In this Letter, we demonstrate another method to enhance USMR at room temperature using a ferromagnetic Ni-Cu alloy. The magnitude of the SF-USMR is improved with the amount of magnons in the FM. Indeed, Borisenko *et al.* have successfully observed the improvement of the USMR ratio with increasing the spin-current-driven magnon population in the NiFe/Pt bilayer [4]. Namely, the FM with a lower T_C is

*yamanoi@phys.keio.ac.jp

more likely to enhance the SF-USMR effect. To investigate how the T_C correlates with the USMR ratio, we measured the USMR ratio for bilayers consisting of Pt and four different transition FMs, i.e., $\text{Ni}_{81}\text{Fe}_{19}$, Ni, $\text{Ni}_{85}\text{Cu}_{15}$, and Fe. The crystalline structures of $\text{Ni}_{81}\text{Fe}_{19}$, Ni, and $\text{Ni}_{85}\text{Cu}_{15}$ are face-centered cubic (fcc), whereas that for Fe is body-centered cubic (bcc). Therefore, similar electronic band structures are expected in the fcc FMs although the number of electrons filling them is different. This Letter describes two observations. First, the USMR ratio is maximized at a particular thickness of FM whose value depends on the nature of the ferromagnetic material. The optimum thickness seems to be consistent with the spin diffusion length (λ_s) which has been reported for each FM. The result suggests that, unlike other MR effects such as GMR and anisotropic MR [22], the USMR effect is caused by spin transfer torque (STT) at the interface between the FM and Pt layers due to the spin Hall-induced spin current in the Pt layer. The second observation is that the maximum USMR ratio for each FM is clearly scaled with T_C . The USMR ratio for $\text{Ni}_{85}\text{Cu}_{15}/\text{Pt}$ is double that of the $\text{Ni}_{81}\text{Fe}_{19}/\text{Pt}$ at room temperature. In comparison, the USMR ratio of Fe/Pt bilayer, whose crystalline structure is bcc, is much lower than the value expected for a fcc FM with a similar T_C value. This result implies that not only the T_C but also the crystalline structure is significant for determining the USMR ratio.

II. SAMPLE PREPARATION AND MEASUREMENT SETUP

The devices consisting of nonmagnetic Pt and FMs, $\text{Ni}_{81}\text{Fe}_{19}$, Ni, $\text{Ni}_{85}\text{Cu}_{15}$, or Fe, were prepared on a thermal oxidized Si substrate by direct current magnetron sputtering. The base pressure was better than 1×10^{-5} Pa. As shown schematically in Figs. 1(a) and 1(b), all bilayers were formed in a standard Hall bar geometry using laser lithography and conventional lift-off techniques. The lateral dimensions for the Hall-bar geometry are $12 \mu\text{m}$ in width and $90 \mu\text{m}$ in length. The thickness of the Pt layer was fixed at 5 nm. The USMR effect was observed by applying an alternating electric current I_{AC} with a frequency $\omega/2\pi = 137$ Hz, along the x axis. The second harmonic of the longitudinal voltage $V_{xx}^{2\omega}$ and transverse voltages $V_{xy}^{2\omega}$ were measured separately using experimental setups as shown schematically in Fig. 1(a) and 1(b), respectively. An external magnetic field swept from -300 to $+300$ mT, whose absolute value was sufficiently large to saturate the magnetization along any in-plane direction. Figures 1(c) and 1(d) show schematically the high- and low-resistance states of the FM/Pt bilayer due to the USMR effect. When an electric current flows in the Pt layer along the x axis, the spin Hall effect generates polarized spin current in the y axis along the z axis. Owing to the USMR effect, the electronic resistance of the FM/Pt bilayer varies depending on the relative orientation of magnetization with respect to the spin polarization of the spin current. As shown in Figs. 1(c) and 1(d), antiparallel and parallel orientations lead to low- and high-resistance states, respectively. Consequently, the USMR effect is expected to be observed in Fig. 1(b) but not in Fig. 1(a). In this Letter, we used the experimental setup shown schematically in Fig. 1(a) to evaluate a property caused by thermal electromotive force in our devices.

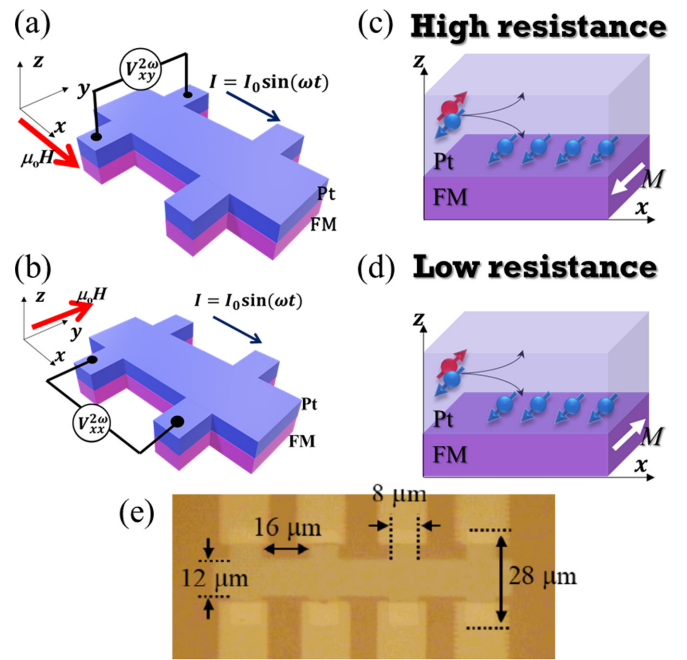


FIG. 1. Schematic experimental setup for measuring the second harmonic of (a) transverse and (b) longitudinal voltages, i.e., $V_{xy}^{2\omega}$ and $V_{xx}^{2\omega}$, with applying external magnetic field along the x and y axes, respectively. Alternating current is always applied along the $+x$ direction. (c) High- and (d) low-resistance states of the FM/Pt bilayer film owing to the USMR effect. (e) Optical microscopic image for our device.

The magnetic properties of monolayers of each FM were measured at temperatures in the range 15–400 K using a superconducting quantum interference device magnetometer, a SQUID MPMS XL from Quantum Design. The T_C of each FM was evaluated from the temperature dependence of the magnetization measured at an external magnetic field of 100 mT. Finally, we discuss the correlation between the T_C and the magnitude of the USMR effect.

III. RESULTS AND DISCUSSION

A. Separate evaluations of thermal electromotive force and USMR effect

Figures 2(a)–2(d) and 2(e)–2(h) show the $V_{xx}^{2\omega}$ and $V_{xy}^{2\omega}$, respectively, as functions of the external magnetic field for the Ni/Pt, $\text{Ni}_{85}\text{Cu}_{15}/\text{Pt}$, $\text{Ni}_{81}\text{Fe}_{19}/\text{Pt}$, and Fe/Pt bilayers. The thicknesses of all the FMs were fixed at 5 nm. As shown in Fig. 2, increases not only in $V_{xx}^{2\omega}$ but also in $V_{xy}^{2\omega}$ were observed for all samples when the polarity of the external magnetic field changed from negative to positive. A magnetization-dependent thermal electromotive force is involved in the change in both $V_{xx}^{2\omega}$ and $V_{xy}^{2\omega}$. The Si substrate situated below the FM/Pt bilayer acted as a heat sink to dissipate the heat [23]. When an electric current was applied to the FM/Pt bilayer along the x axis, a temperature gradient was produced in the ferromagnetic layer along the z axis. According to the anomalous Nernst effect (ANE) [24], a thermal electromotive force appears perpendicularly to both the thermal gradient and the magnetization in the FM. Namely, the ANE appears in

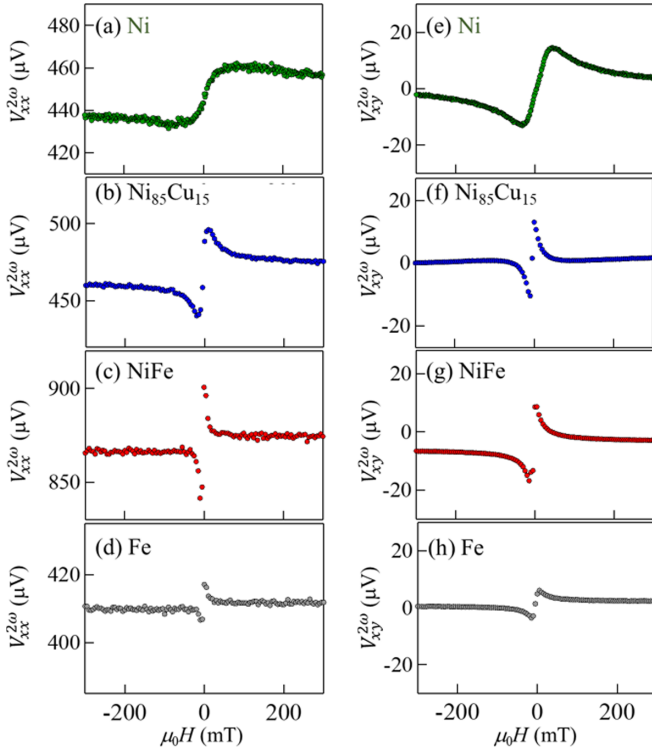


FIG. 2. Magnetic field dependence of $V_{xx}^{2\omega}$ and $V_{xy}^{2\omega}$ for (a), (e) Ni/Pt, (b), (f) $\text{Ni}_{85}\text{Cu}_{15}$ /Pt, (c), (g) $\text{Ni}_{81}\text{Fe}_{19}$ /Pt, and (d), (h) Fe/Pt bilayers. The current density j_c was fixed at $0.87 \times 10^{11} \text{ A/m}^2$.

both $V_{xx}^{2\omega}$ and $V_{xy}^{2\omega}$ although the USMR effect appears only in $V_{xx}^{2\omega}$. Typically, the thermal electromotive force in the $V_{xx}^{2\omega}$ was evaluated from the value of $V_{xy}^{2\omega}$ using the ratio of distance between voltage terminals as a geometric correction.

To evaluate the thermal electromotive force in $V_{xx}^{2\omega}$ correctly from the value of $V_{xy}^{2\omega}$, we measured $V_{xx}^{2\omega}$ and $V_{xy}^{2\omega}$ for a $\text{Ni}_{81}\text{Fe}_{19}$ monolayer, where only the ANE appears. Thus, we can examine the ratio of the thermal electromotive forces in $V_{xx}^{2\omega}$ and $V_{xy}^{2\omega}$ in the device geometry used for observing the USMR effect. The SOT produced by the spin current in the Pt layer also affects the value of $V_{xy}^{2\omega}$. This SOT-induced component of $V_{xy}^{2\omega}$ is usually in proportion to the magnetic susceptibility of the ferromagnetic layer. The SOT-induced voltage can therefore be neglected under a strong magnetic field, whereas the ANE-induced voltage is independent of the strength of the magnetic field [3,25].

Figures 3(a) and 3(b) show the magnetic field dependence of $V_{xx}^{2\omega}$ and $V_{xy}^{2\omega}$ for the $\text{Ni}_{81}\text{Fe}_{19}$ monolayer. A rapid increase in $V_{xx}^{2\omega}$ and $V_{xy}^{2\omega}$ due to the ANE in the $\text{Ni}_{81}\text{Fe}_{19}$ film was clearly observed when the magnetic field was reversed, although the increase in $V_{xy}^{2\omega}$ was much larger than in $V_{xx}^{2\omega}$. From the sign of the Nernst coefficient for $\text{Ni}_{81}\text{Fe}_{19}$ [24], the rapid increases in $V_{xx}^{2\omega}$ and $V_{xy}^{2\omega}$ suggest that there was a flow of Joule heating toward the Si substrate. This indicates that the Si substrate acted as a heat sink. Figure 3(c) shows the current density dependence of the voltage increase, $\Delta V_{xx}^{2\omega}$ and $\Delta V_{xy}^{2\omega}$, which are defined as the difference between the averaged value from -200 to -300 mT and that from $+200$ to $+300$ mT for $V_{xx}^{2\omega}$ and $V_{xy}^{2\omega}$, respectively. As shown by

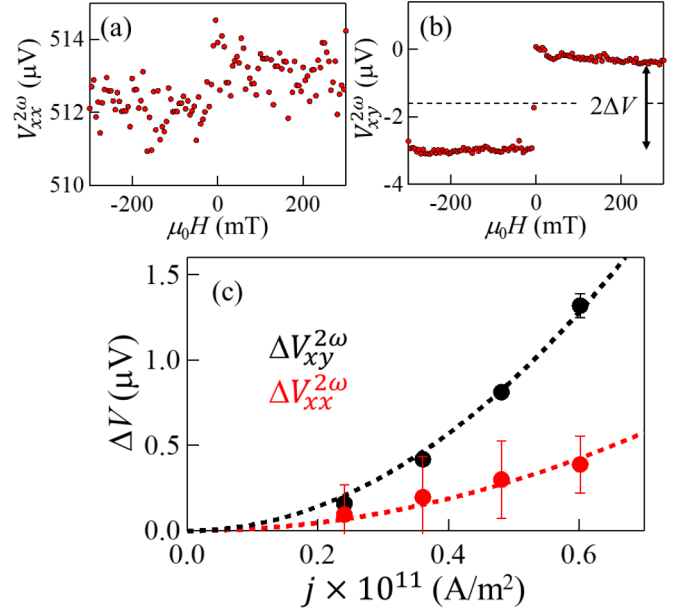


FIG. 3. Magnetic field dependence of (a) $V_{xx}^{2\omega}$ and (b) $V_{xy}^{2\omega}$ for the $\text{Ni}_{81}\text{Fe}_{19}$ monolayer. A current density j_c was fixed at $0.60 \times 10^{11} \text{ A/m}^2$. (c) $\Delta V_{xx}^{2\omega}$ and $\Delta V_{xy}^{2\omega}$ for $\text{Ni}_{81}\text{Fe}_{19}$ monolayer as a function of the electric current density. Black and red dashed curves are the best fit results with a quadratic function. The error bars are systematic errors estimated by the measurement device accuracy.

the dashed lines in Fig. 3(c), both $\Delta V_{xx}^{2\omega}$ and $\Delta V_{xy}^{2\omega}$ increase exponentially with respect to the electric current density. Such an exponential relationship clearly suggests that the $\Delta V_{xx}^{2\omega}$ and $\Delta V_{xy}^{2\omega}$ are caused by the Joule heating, whose amplitude is also exponentially related to the electric current density j . The ratio of the amplitude of $\Delta V_{xx}^{2\omega}$ to that of $\Delta V_{xy}^{2\omega}$ was found to be 0.40. This value is essential to separately evaluate the thermal electromotive force and the USMR effect in $V_{xx}^{2\omega}$ for the FM/Pt bilayer. The temperature gradient seen in the FM/Pt bilayer was similar to that seen in the $\text{Ni}_{81}\text{Fe}_{19}$ monolayer because the lateral size of the bilayer in the device is much larger than its thickness.

Finally, we can separate the contributions to the thermal electromotive force $\Delta V_{xx}^{\text{ANE}}$ and the USMR effect $\Delta V_{xx}^{\text{USMR}}$ in $\Delta V_{xx}^{2\omega}$. As mentioned previously, we found that $\Delta V_{xx}^{\text{ANE}} = 0.33\Delta V_{xy}^{2\omega} = 0.33\Delta V_{xx}^{2\omega}$. Consequently, the contribution of the USMR effect in $\Delta V_{xx}^{2\omega}$ is given by

$$\Delta V_{xx}^{\text{USMR}} = \Delta V_{xx}^{2\omega} - 0.33\Delta V_{xy}^{2\omega}. \quad (1)$$

Figure 4 shows the j dependence of R_{ANE}/R and R_{USMR}/R for the $\text{Ni}_{81}\text{Fe}_{19}$ /Pt bilayer, where R_{ANE} and R_{USMR} are given by $\Delta V_{xx}^{\text{ANE}}/I$ and $\Delta V_{xx}^{\text{USMR}}/I$, respectively. Here, I is the injected current, and R is the averaged resistivity of the $\text{Ni}_{81}\text{Fe}_{19}$ /Pt bilayer. The linear increase in R_{USMR}/R with respect to j is attributed to the strength of the SD scattering at the FM/Pt interface, which is proportional to the magnitude of spin current produced in the Pt layer. As shown in Fig. 4, R_{ANE}/R also increased linearly with j , which can be explained by assuming that the temperature gradient in the ferromagnetic layer is proportional to j^2 .

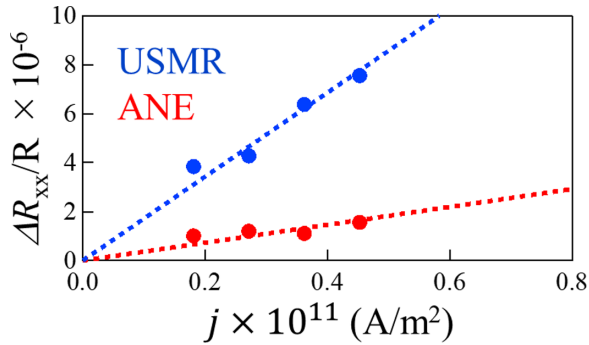


FIG. 4. j dependence of R_{USMR}/R and R_{ANE}/R for the $\text{Ni}_{81}\text{Fe}_{19}/\text{Pt}$ bilayer.

B. Curie temperature dependence of the USMR effect

To discuss the relationship between the USMR ratio and T_C , we examined the value of T_C for each ferromagnetic monolayer by measuring the variation of magnetization with temperature. Figure 5(a) shows the temperature dependence of saturation magnetization M_s measured at an in-plane

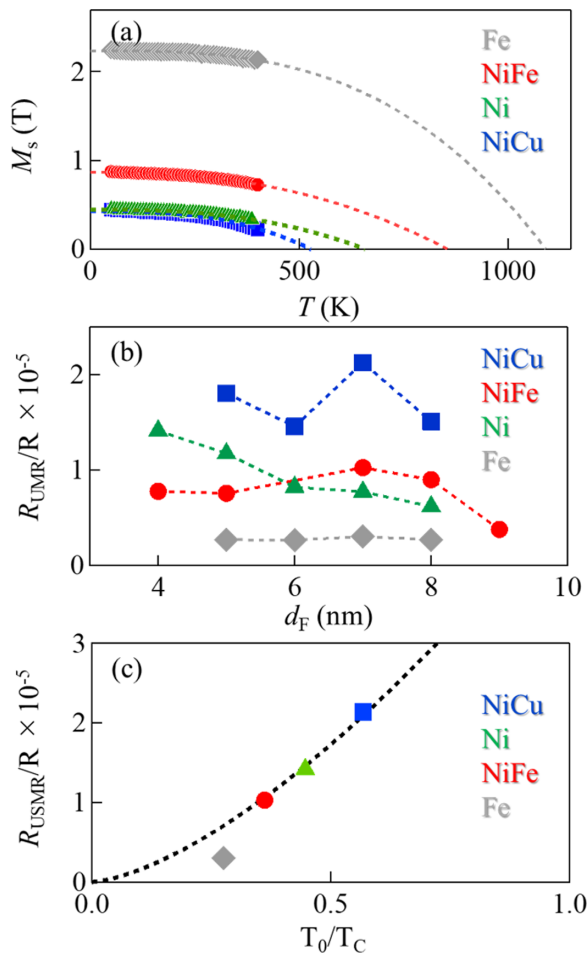


FIG. 5. (a) Temperature dependence of the magnetization for each FM film. (b) FM thickness dependence of R_{USMR}/R . (c) Curie temperature dependence of R_{USMR}/R for the FM/Pt bilayer. The dashed line is the fitting curve using $R_{\text{USMR}}/R = A(T_0/T_C)^\alpha$. Here, A and α are the proportionality constant and exponent, respectively.

magnetic field of 100 mT. To evaluate the value of T_C , the variation of M_s with temperature was fitted using the equation $M_s(T)/M_s(0) = 1 - (T/T_C)^\alpha$, where $M_s(0)$ and α are the M_s at $T = 0$ K and exponent, respectively [23,26]. After finding the best fit with this equation, we obtained T_C values as 527, 659, 854, and 1090 K for $\text{Ni}_{85}\text{Cu}_{15}$, Ni, $\text{Ni}_{81}\text{Fe}_{19}$, and Fe monolayers with a thickness of 5 nm, respectively. The $M_s(0)$ values were also evaluated as 0.43, 0.41, 0.87, and 2.2 T for each FM, respectively. The evaluated $M_s(0)$ values are consistent with those expected from the Slater-Pauling curve [27].

Figure 5(b) shows R_{USMR}/R as a function of thickness of each FM. Here, the current density j was fixed at 1×10^{11} A/m². As shown in Fig. 5(b), the observed USMR ratio was positive for all devices, which is attributed to the fact that the USMR effect is caused by the spin current generated in the Pt layer whose spin Hall angle is positive [1,3,23,28]. In the case of the SD-USMR effect, variation in electric resistivity occurs only in the region of the FM where a nonequilibrium spin accumulation appears. Such a spin accumulation decays depending on the λ_s from the FM/Pt interface. Consequently, the SD-USMR effect is maximized when the FM thickness coincides with λ_s [5]. In the case of SF-USMR, variation in electric resistivity occurs in the region of the FM where a nonequilibrium magnon is excited. Such a magnon excitation is attributed to the STT caused by the injection of spin current from the Pt layer. The strength of the STT also decays in proportion with the distance from the FM/Pt interface. Therefore, the resistance change due to the SF-USMR effect is maximized when the FM thickness is consistent with the λ_s of the FM. Indeed, as shown in Fig. 5(b), R_{USMR}/R for the $\text{Ni}_{81}\text{Fe}_{19}/\text{Pt}$ bilayer is maximized when the FM thickness is 7 nm, which is similar to the value of λ_s reported for $\text{Ni}_{81}\text{Fe}_{19}$ at room temperature (5.2 nm) [29]. Unfortunately, we could not make FMs thinner than 4 nm owing to degradation of the magnetic properties of FMs in our sputtering system. The value of R_{USMR}/R measured for 4-nm-thick Ni is regarded as the approximate maximum USMR effect for a Ni/Pt bilayer.

Figure 5(c) shows the maximum USMR ratio as a function of the reciprocal of T_C . Here, T_0 is 300 K. As shown in Fig. 5(c), the maximum USMR ratio is enhanced as T_C approaches T_0 . The maximum USMR ratio can be doubled by changing the FM from $\text{Ni}_{81}\text{Fe}_{19}$ ($T_C = 854$ K) to $\text{Ni}_{85}\text{Cu}_{15}$ ($T_C = 527$ K). As shown by the dashed curve in Fig. 5(c), except for the Fe/Pt bilayer, the maximum USMR ratio can be explained by a function of three-halves power of $(T_0/T_C)^{3/2}$ even though different FMs are attached to the Pt layer. Such a T_C dependence of the maximum USMR ratio can be explained by considering that SF-USMR is typically dominant at room temperature [2,6]. According to the spin-wave theory for ferromagnetic materials, the number of thermally excited magnons is proportional to the $(T/J)^{3/2}$, where T is the temperature of the FM and J is the strength of exchange coupling. Generally, the magnitude of J is proportional to the T_C of the FM. Therefore, the magnitude of the SF-USMR is expected to be in proportion to $(T/T_C)^{3/2}$ as shown in Fig. 5(c). However, the maximum USMR ratio for the bcc Fe/Pt bilayer is much lower than the $(T_0/T_C)^{3/2}$ tendency which is appropriate for other fcc FMs. This discrepancy may be due to the difference in the SD-USMR effect between fcc and bcc FMs. Generally,

the electron band structure is highly dependent on the crystalline structure of the FM. In the case of the SD-USMR, the density of state for spin subbands determines the strength of SD scattering. These results indicate that using a low T_C fcc FM is a potential method to improve the USMR ratio for a FM/Pt-based bilayer at room temperature. In addition, it is advantageous to use an efficient spin-electron conversion material as the nonmagnetic layer in the FM/NM bilayer.

IV. CONCLUSION

We demonstrated enhancement of the USMR effect at room temperature by lowering the T_C of the FM in the FM/NM bilayer. The magnitude of the room-temperature USMR effect for bilayers consisting of FMs and Pt was in proportion to $(T_0/T_C)^{3/2}$ for all bilayers tested apart from Fe/Pt. This relationship is explained by the fact that the room-temperature USMR effect is dominated by the SF-USMR effect, which depends on the amount of incoherent magnons, and by the relationship between the T_C and the

incoherent magnons according to the spin-wave theory. Therefore, the strength of the USMR effect at room temperature reflects the T_C dependence of the proportion of thermally excited magnons. The maximum USMR ratio for the bcc Fe/Pt bilayer was much lower than the expected $(T_0/T_C)^{3/2}$ value found for the fcc FM/Pt bilayers. This discrepancy in the USMR effect between fcc and bcc FMs may be due to the difference in the magnitude of the SD-USMR effect. Since the density of states in the spin subbands determines the strength of the SD scattering, the USMR effect differs depending on the crystal structure of the FM layer. We believe that our findings will increase the understanding of electron transport in spin-current-driven magnetic systems and contribute to the design of next-generation MR applications.

ACKNOWLEDGMENTS

This work was partially supported by JSPS KAKENHI Grant No. JP18H03867, JST CREST Grant No. JPMJCR19J4, Grant-in-Aid for Research Activity start-up No. 19K23588, and The Murata Science Foundation, Japan.

-
- [1] *Spin Current*, edited by S. Maekawa, S. O. Valenzuela, E. Saitoh, and T. Kimura, Series on Semiconductor Science and Technology (Oxford University Press, Oxford, U.K., 2017).
- [2] C. O. Avci, J. Mendil, G. S. D. Beach, and P. Gambardella, *Phys. Rev. Lett.* **121**, 087207 (2018).
- [3] C. O. Avci, K. Garello, A. Ghosh, M. Gabureac, S. F. Alvarado, and P. Gambardella, *Nat. Phys.* **11**, 570 (2015).
- [4] I. Borisenko, V. Demidov, S. Urazhdin, A. Rinkevich, and S. Demokritov, *Appl. Phys. Lett.* **113**, 062403 (2018).
- [5] S. S.-L. Zhang and G. Vignale, *Phys. Rev. B* **94**, 140411(R) (2016).
- [6] K.-J. Kim, T. Li, S. Kim, T. Moriyama, T. Koyama, D. Chiba, K.-J. Lee, H.-W. Lee, and T. Ono, *Appl. Phys. Express* **12**, 063001 (2019).
- [7] J. E. Hirsch, *Phys. Rev. Lett.* **83**, 1834 (1999).
- [8] J. Sinova, S. O. Valenzuela, J. Wunderlich, C. H. Back, and T. Jungwirth, *Rev. Mod. Phys.* **87**, 1213 (2015).
- [9] Y. K. Kato, R. C. Myers, A. C. Gossard, and D. D. Awschalom, *Science* **306**, 1910 (2004).
- [10] E. Saitoh, M. Ueda, H. Miyajima, and G. Tatara, *Appl. Phys. Lett.* **88**, 182509 (2006).
- [11] T. Kimura, Y. Otani, T. Sato, S. Takahashi, and S. Maekawa, *Phys. Rev. Lett.* **98**, 156601 (2007).
- [12] G. Binasch, P. Grünberg, F. Saurenbach, and W. Zinn, *Phys. Rev. B* **39**, 4828 (1989).
- [13] M. N. Baibich, J. M. Broto, A. Fert, F. Nguyen Van Dau, F. Petroff, P. Etienne, G. Creuzet, A. Friederich, and J. Chazelas, *Phys. Rev. Lett.* **61**, 2472 (1988).
- [14] L. Liu, A. Richardella, I. Garate, Y. Zhu, N. Samarth, and C.-T. Chen, *Phys. Rev. B* **91**, 235437 (2015).
- [15] A. Dankert, J. Geurs, M. V. Kamalakar, S. Charpentier, and S. P. Dash, *Nano Lett.* **15**, 7976 (2015).
- [16] K. Kondou, R. Yoshimi, A. Tsukazaki, Y. Fukuma, J. Matsuno, K. Takahashi, M. Kawasaki, Y. Tokura, and Y. Otani, *Nat. Phys.* **12**, 1027 (2016).
- [17] N. H. Duy Khang and P. N. Hai, *J. Appl. Phys.* **126**, 233903 (2019).
- [18] Y. Lv, J. Kally, D. Zhang, J. S. Lee, M. Jamali, N. Samarth, and J.-P. Wang, *Nat. Commun.* **9**, 111 (2018).
- [19] M. Cubukcu, O. Boulle, M. Drouard, K. Garello, C. Onur Avci, I. Mihai Miron, J. Langer, B. Ocker, P. Gambardella, and G. Gaudin, *Appl. Phys. Lett.* **104**, 042406 (2014).
- [20] F. Oboril, R. Bishnoi, M. Ebrahimi, and M. B. Tahoori, *IEEE Trans. Comput.-Aided Des. Integr. Circuits Syst.* **34**, 367 (2015).
- [21] K. Hasegawa, T. Koyama, and D. Chiba, *Phys. Rev. B* **103**, L020411 (2021).
- [22] T. McGuire and R. Potter, *IEEE Trans. Magn.* **11**, 1018 (1975).
- [23] P. Phu, K. Yamanoi, K. Ohnishi, J. Hyodo, K. Rogdakis, Y. Yamazaki, T. Kimura, and H. Kurebayashi, *J. Magn. Magn. Mater.* **485**, 304 (2019).
- [24] R. Bennet, A. Hojem, and B. Zink, *AIP Adv.* **10**, 065127 (2020).
- [25] C. O. Avci, K. Garello, M. Gabureac, A. Ghosh, A. Fuhrer, S. F. Alvarado, and P. Gambardella, *Phys. Rev. B* **90**, 224427 (2014).
- [26] K.-M. Lee, J. W. Choi, J. Sok, and B.-C. Min, *AIP Adv.* **7**, 065107 (2017).
- [27] T. Mashimo, X. Huang, X. Fan, K. Koyama, and M. Motokawa, *Phys. Rev. B* **66**, 132407 (2002).
- [28] W. Zhang, W. Han, X. Jiang, S.-H. Yang, and S. S. P. Parkin, *Nat. Phys.* **11**, 496 (2015).
- [29] G. Zahnd, L. Vila, V. T. Pham, M. Cosset-Cheneau, W. Lim, A. Brenac, P. Laczkowski, A. Marty, and J. P. Attané, *Phys. Rev. B* **98**, 174414 (2018).